Renewed characterization of a Mach 6 hypersonic wind tunnel

Sacha Hirsch, Guillaume Grossir, Olivier Chazot

Renewed characterization of a Mach 6 hypersonic wind tunnel

Sacha Hirsch*
ONERA, Palaiseau, 91123, France

Guillaume Grossir† and Olivier Chazot‡
von Karman Institute for Fluid Dynamics, Sint-Genesius-Rode, 1640, Belgium

This paper presents a renewed characterization of a Mach 6 hypersonic wind tunnel. The H3 hypersonic facility, located at the von Karman Institute, is a blowdown-type wind tunnel with a useful test duration of the order of one second to one minute, currently equipped with a fixed-Mach, axisymmetric contoured nozzle. The H3 is a "cold" hypersonic wind tunnel, achieving high Mach numbers by lowering the speed of sound; it aims to replicate the Reynolds and Mach numbers commonly encountered by hypersonic vehicles in-flight. A test campaign assessing the full envelope of the testing conditions of the H3 is carried out. Some tests are performed at low reservoir temperatures to characterize the onset of condensation experimentally. For the first time, the free-stream static pressure in the H3 is assessed directly by the agency of a so-called Nagamatsu probe designed and optimized for operation within the facility. The impact pressure is measured with a classic Pitot probe. Free-stream Pitot and static pressures are measured simultaneously, along with reservoir pressure and temperature. Furthermore, the behavior of the flow around the probes is visualized via schlieren photography with a high-speed camera; the resulting pictures are used inter alia to retrieve the free-stream Mach number. CFD simulations of the flow in the H3 nozzle and around the static pressure probe are used to correct the data for viscous interaction effects. Then, different rebuilding techniques are implemented and critically compared to each other. The Mach number estimated from the static pressure probe output was found to be consistently inferior to the classical Pitot probe estimate, which could either be explained by the presence of non-isentropic phenomena in the nozzle or by a systematic error in the probe calibration, in particular in the viscous correction of the measured pressure. Nevertheless, the onset of condensation was detected successfully for operation with low stagnation temperatures.

I. Nomenclature

$\Delta t_{particle}$	=	Flight time of a fluid particle in the test section [s]
Δt_{tunnel}	=	Test duration [s]
ϵ	=	Probe wall rugosity [µm]
γ	=	Polytropic coefficient
Kn	=	Knudsen number
l	=	Horizontal length of the last characteristic line stemming from the nozzle axis entirely contained in the nozzle [m]
M	=	Mach number
μ	=	Dynamic viscosity [Pa.s]
P	=	Pressure [Pa or bar]
Re	=	Unit Reynolds number [m^{-1}]
T	=	Reservoir temperature [K]
u	=	Flow speed [m/s]
Y_{shock}	=	Distance of the shock from the static pressure probe axis at a given abscissa [mm]
x	=	Abscissa along the nozzle or the probe axis [m]
$\bar{\chi}$	=	Viscous interaction parameter

*PhD. Candidate, DMPE, sacha.hirsch@onera.fr
†Research Engineer, Aeronautics and Aerospace Department, guillaume.grossir@vki.ac.be
‡Head and Professor, Aeronautics and Aerospace Department, olivier.chazot@vki.ac.be

Subscripts

atm	=	Atmospheric quantity
0	=	Reservoir quantity
∞	=	Free-stream quantity
$t2$	=	Total quantity behind a bow shock in the free stream (i.e. Pitot/impact quantity)
wall	=	Quantity at the static pressure probe wall

II. Introduction

The accurate determination of the free-stream conditions in a wind tunnel is essential to the interpretation and reliability of the experiments conducted within it. For hypersonic wind tunnels with short test durations, these quantities are not easily accessible, and therefore must be reconstructed from a reduced number of variables obtained through direct measurements. The classical simplified models for compressible fluid dynamics show that only three quantities (for example free-stream total pressure, reservoir pressure, and temperature) are needed to fully characterize the flow. Additional measurements within the flow allow to over-constrain the system and cross-check the consistency of the dataset as well as the validity of the underlying assumptions.

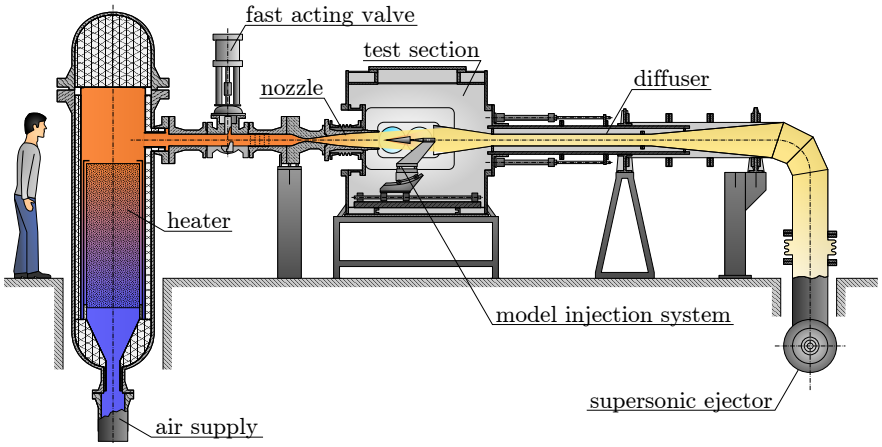

Fig. 1 Sketch of the VKI H3 hypersonic blow-down tunnel

Recent investigations by Grossir & al. [1] in the Longshot facility, the gun-type Mach 11 wind tunnel of the von Karman Institute, showed a strong discrepancy between the expected value of the static pressure computed with a reconstruction model and the value gauged directly with a free-stream static pressure probe, also called a Nagamatsu probe. Several hypotheses were put forward to explain this inconsistency; condensation effects have been ruled out but other interpretations still require experimental testing. While a study is ongoing on the Longshot tunnel itself using non-intrusive measurement techniques, a parallel project on the H3 wind tunnel has been undertaken, using, by contrast, intrusive pressure probes. It is believed that using the same probe that was used in [1] within the H3 wind tunnel could help to validate or reject some of those hypotheses. The H3 Mach 6 nozzle was designed in the 1970s, and has undergone many characterization campaigns; however, the only free-stream pressure sensors used in those test campaigns were always Pitot (impact) probes, for example in [2].

Furthermore, the complete operating map of the H3 wind tunnel remains only partially known. In particular, the condensation limit, below which the nitrogen molecules become liquid, has not been characterized experimentally.

Flow rebuilding

To characterize the free-stream flow of a hypersonic wind tunnel, Grossir designed a static pressure probe. The probe is placed in the test section of the tunnel, along with a classic Pitot probe and a heat flux probe. The measurement of free-stream static pressure P_{wall}, Pitot pressure P_{t2} and stagnation heat flux Q allows for full flow characterization, using an iterative algorithm. This algorithm uses the equation of Fay and Riddell for the heat flux in a hypersonic flow

around a hemispherical object [3]. The flow quantities derived with this method are then compared to the expected quantities computed using reservoir measurements and an algorithm assuming an isentropic and adiabatic expansion through the nozzle. A good agreement between the two methods means that those assumptions are realistic.

The combination of three probes used by Grossir in [1] is not the only option for direct or quasi-direct test section flow characterization. Several other probes can be used together, for example, double hot-wire and Pitot. In the current test campaign, the chosen free-stream sensors are a static pressure probe and a Pitot probe. A temperature or heat flux probe might be eventually added in further investigations, but at first, the two pressure probes in combination with the reservoir probes can theoretically validate the isentropic expansion hypothesis.

Condensation phenomenon

For some operating points at sufficiently low temperatures and high enough pressures, air molecules can liquefy while undergoing expansion in the nozzle. However, due to the high expansion rate, the liquid droplets can sometimes appear at lower temperatures than expected. This phenomenon is known as supercooling, and Daum & Gyarmathy provide a complete theoretical and empirical model to predict its yield [4].

To detect the condensation onset experimentally, several procedures are described in the literature. Daum [5] used a single Pitot probe to measure the impact pressure (*i.e.* total pressure behind a bow shock). The stagnation pressure in the reservoir is held constant, while the stagnation temperature is slowly decreased. The onset of condensation is defined as a sudden change in impact pressure.

Wegener [6] shows that condensation has effects on a lot of different quantities in the flow, in particular the free-stream static pressure. Since this quantity is nearly directly measured by the Nagamatsu probe, the condensation onset can be detected that way. Thus, the static pressure probe could be used in combination with the impact pressure probe to detect condensation reliably.

An analogous method has been used in the Longshot wind tunnel by Grossir & al [1]; both the impact pressure and static pressure measurement are used to reconstruct the free-stream temperature. When lowering the stagnation temperature of the Longshot by tuning the compression process, the free-stream temperature eventually reaches a plateau: this is the condensation point. A similar method will be used in this investigation.

The remaining of this paper is structured as follows. Section III.A will give a detailed overview of the hardware used during the test campaign, the output of which is corrected by CFD simulations presented in section III.B. The algorithms used to confront the output of each probe to the isentropic assumption and other models are presented in section III.D. The existing analytical and empirical models for condensation within a hypersonic wind tunnel nozzle, as well as the chosen method for its experimental detection, are presented in section III.E. A rundown of the uncertainty estimation method is presented in section III.F. Results are presented and discussed in sections IV.A et seq. Finally, conclusions and perspectives are presented in section V.

III. Methodology

A. Sensor description and configuration

1. Static pressure probe

The first static pressure probe for hypersonic flows was designed by Nagamatsu & al. [7]. Many iterations exist on this probe design. However, a robust and complete design is described in [1]. Its geometry is a needle-like body, facing the flow, linked to the test stand with an ogival or conical wider afterbody. The measurement holes must be far enough from the tip of the needle to be outside the over-pressure zone created by the ogival head, and far enough from the afterbody and test stand to avoid recirculation effects. However, even with those precautions, the pressure measured by the piezoelectric sensor must be corrected for viscous effects (by a factor of a few percent) with a 2D, finite volume simulation of the flow around the probe. Ideally, the probes built for the Longshot wind tunnel [1] could have been reused for the H3 characterization. However, the form factor of those probes is too large for the H3 test section. Thus, a new probe was designed and built, using the previous design as an inspiration. A general view of the probe designed for the H3 is shown in figure 2a; it is entirely built with stainless steel with a needle diameter of 5 mm and an overall length of 204mm. The nose is a 10° cone with a hemispherical tip. This shape is smoothly linked to the probe cylindrical body with a polynomial of the fourth degree. The cylindrical part of the probe is comprised of two identical hollow tubes mounted together with a linkage part within which a Kulite XCQ-080-5 pressure sensor is inserted. The

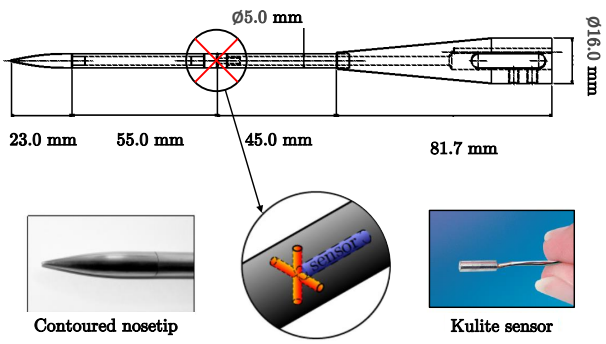

(a) Schematic of the free-stream static pressure probe designed for the H3 wind tunnel.

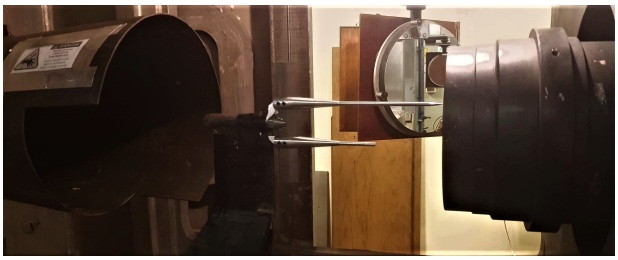

(b) Static pressure probe (top) and Pitot probe (bottom), mounted on their stand. In the final configuration, the test stand as well as the wires and compensation modules of the sensors are covered in aluminum tape to dissipate heat and protect the sensor cables

Fig. 2 Static pressure probe schematic (a) and picture of the probe configuration in the wind tunnel (b)

cables of the sensor run in the hollow tube connected to the base. The base itself is made of a 10 degrees hollow cone and a cylindrical part used to mount the probe on its test stand. Such a slender profile prevents any boundary layer separation along the needle and thus ensures that the flow perturbation induced by the base does not influence the pressure measurement upstream.

2. Pitot probe

The Pitot probe is used to measure the impact pressure in the test section. Such probes are employed quasi-systematically when calibrating a wind tunnel; most of the time, multiple Pitot tubes are arranged in a rake [2] to map the entire test section, but this will not be useful for the current campaign. The design of such a probe is relatively straightforward: a piezoelectric pressure sensor embedded in an open stainless steel tube suffices. The outer tube has a 5 mm diameter; the head is a straight cylinder. This probe is fitted with a Kulite XCE-093-50 sensor.

A view of the probes mounted on their stand is shown in figure b. The stand itself has a slender profile, to avoid any perturbation of the flow around the probes. The probes are placed so that the tip of the static pressure probe is at the nozzle exit and that both sensors are at the same horizontal position. The signal of the sensors is fed into a pressure conditioner, the output of which is read using a NI-9205 acquisition card. Both probes are calibrated before and after the test campaign using the Longshot tunnel vacuum chamber, against an MKS 626C transducer for pressures below 1.6 kPa and a Ceravac CTR-100 for higher pressures.

3. Reservoir Probes

Two probes are mounted in the reservoir of the H3. The pressure sensor is a WIKA S-20. Its signal is directly fed to the NI-9205 acquisition card. The temperature sensor is a type-K thermocouple, mounted in a cylindrical tube aligned with the flow. The voltage of the thermocouple is amplified and read by a NI-9212 acquisition card. While the pressure sensors data was acquired at 2kHz, the thermocouple data could only be sampled at 95 Hz.

4. Other measurements

A schlieren apparatus, embedded in the H3, is used in combination with a Phantom Miro M310 high-speed camera and a LED light source. It is used to get independent confirmation of the Mach number through the measurement of the angle of the shock generated, for example, by a static pressure probe [1]. With this technique, one can also check that the probes do not interfere with each other when close together. Finally, in case of defects in the probe design and manufacturing, an unwanted separation of the boundary layer or instabilities in the flow around the probes can be detected. Depending on the runs, different image acquisition rates and shutter speeds were used. Also, the aperture of a diaphragm placed in front of the light source was tweaked over the course of the test campaign to obtain a light source as punctual as possible while letting sufficient light through. An example of the schlieren visualization is presented in figure 3.

Finally, since the tunnel cannot start up with an object in the alignment of the nozzle axis, the probes are injected after the establishment of the hypersonic flow, using a pneumatic jack. The typical injection time is between 0.1 and 0.2

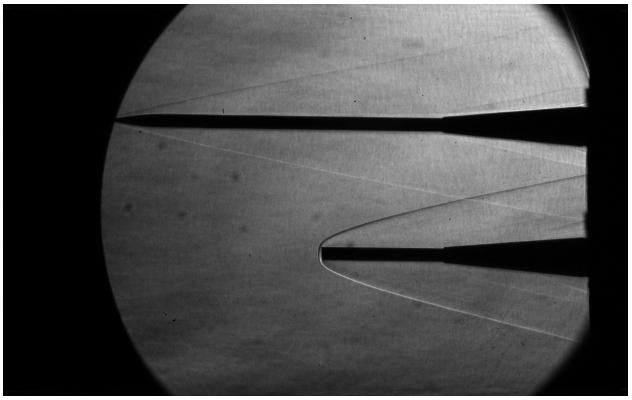

Fig. 3 Schlieren visualization of the flow around the two pressure probes inside the H3 Mach 6 wind tunnel. The static pressure probe is on the top and the Pitot probe is on the bottom. This particular test run was performed at $P_0 = 20.66$ bars and $T_0 = 500.6$K

s. Its limit switch signal is used to delineate the useful time window for data analysis.

B. Numerical simulations

The static pressure probe measurement P_{wall} cannot be directly assimilated to the free-stream pressure P_∞. Viscous effects have to be taken into account. Even if the assumption is made that pressure is constant in the boundary layer over the sensor intake, the interaction between the boundary layer and the inviscid flow above it makes it necessary to correct the measured data with Reynolds, Mach, and temperature. Behrens [8] uses the Pi-Buckingham approach to design a viscous interaction parameter for such probes:

$$\frac{P_\infty}{P_{\text{wall}}} = 1 + A\bar{\chi} + B\bar{\chi}^2 + ... \tag{1}$$

with $\bar{\chi}$ the viscous interaction parameter:

$$\bar{\chi} = M^3\sqrt{\frac{C}{Re_\infty}} \tag{2}$$

where

$$C = \frac{\mu_{wall}T_\infty}{\mu_\infty T_{wall}}$$

Second-order CFD simulations of the static pressure probe were performed using the commercial software Metacomptech CFD++ to estimate the pressure over the probe surface. The configuration of the problem allows for a 2D axial symmetry geometry. To ensure a sufficiently fine spatial resolution of the problem (in particular near the wall) while keeping the computational complexity to a minimum, only the flow in proximity to the probe is considered; a few trial and error cycles are performed to keep the shock within the computational domain. The mesh is structured with quadrilateral cells and spatially converged; it is presented in figure 5. The long useful test duration of the H3 wind tunnel ($\Delta t_{particle} < 10^{-3}\Delta t_{tunnel}$) allows to neglect any transient phenomenon and thus the simulations are run in steady mode. The fluid is dry air.

The flow is compressible given the high Mach numbers considered. A perfect gas equation of state is used to model molecular interactions. Given the low temperatures in the test section and the low Knudsen number ($4.10^{-6} < \text{Kn}_\infty = \frac{\text{M}}{\text{lRe}_\infty}\sqrt{\frac{\gamma\pi}{2}} < 3.10^{-5}$ over the test envelope), this assumption should be realistic.

The flow is considered to be viscous and laminar. The low manufacturing tolerances of the probe (rugosity $\epsilon \leq 1.6$ µm) and its very slender design should ensure that no transition to turbulence is triggered in the boundary layer, at least before the conical base. Finally, the probe surface is considered isothermal. This is verified a posteriori by checking that the time variation of the static pressure readings is negligible.

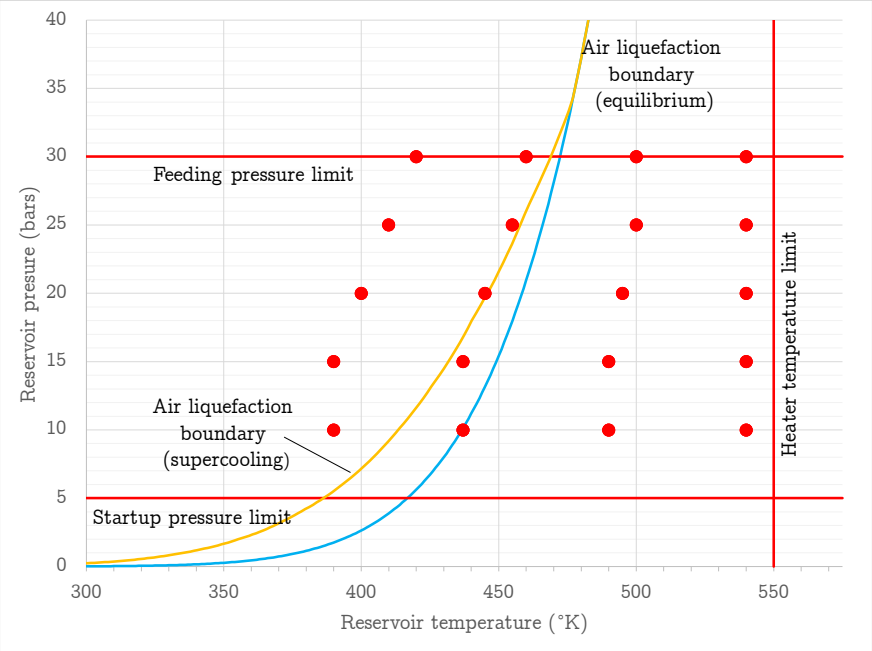

Fig. 4 Map of the CFD simulations inputs, marked as red dots. Each dot corresponds to three simulations, at the reservoir pressure and temperature defined by its position on the plane and at respective Mach numbers M = 5.9, M = 6.0, and M = 6.1. Limits of the test envelope (see section III.F) are also displayed.

1. Viscous correction

Three input quantities are needed to accurately compute the viscous correction needed for each experimental data point : free-stream pressure, free-stream temperature and free-stream Mach number. However, no direct measurements of free-stream temperature nor Mach number are performed during the current campaign; and the free-stream pressure measurement is itself dependent on the computation of the viscous interaction parameter. The algorithm needed to compute those input parameters is iterative (see section III.E). Therefore, more than one simulation per experimental data point are needed, as running one or more simulation for each iteration of the algorithm would be obviously too costly; consequently an alternate solution has been designed.

A series of 60 CFD simulations mapping the whole test envelope of the H3 have been performed. Each simulation is characterized by its free-stream pressure, free-stream temperature, and Mach number provided in its input. Those simulations are mapped on a reservoir pressure, temperature plane on figure 4. We can then define a linear interpolation $\frac{P_{\text{wall}}}{P_\infty}(P_\infty, T_\infty, M)$ of the the viscous correction coefficients obtained in the output of those simulations. This function can be evaluated quickly and thus used in the iterative algorithm. A sample of the viscous correction coefficients

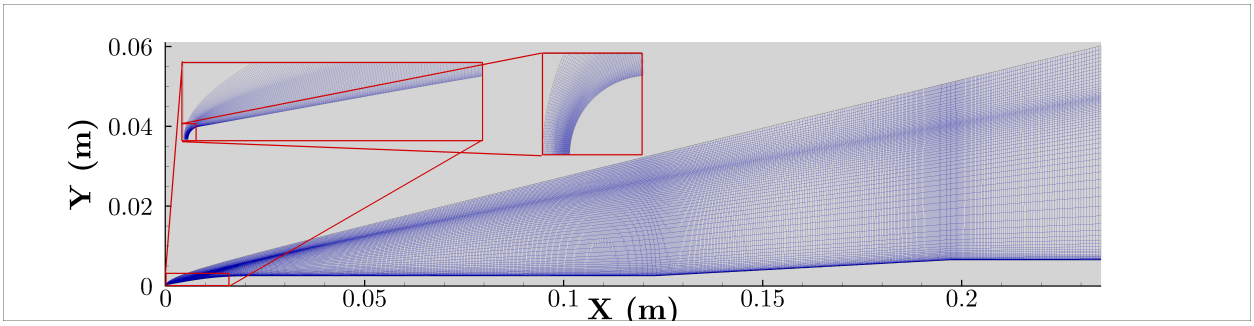

Fig. 5 View of the mesh used for simulating the flow around the probe. Insets show the detail of the mesh near the nose tip facing the flow.

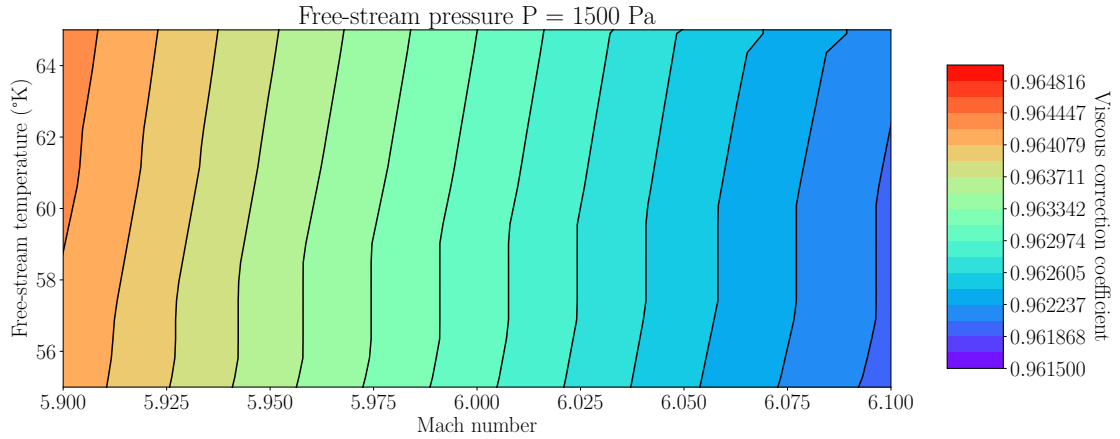

Fig. 6 Dependence of the viscous correction coefficient $\frac{P_{wall}}{P_\infty}$ with free-stream temperature and Mach number at P_∞ = 1500 Pa.

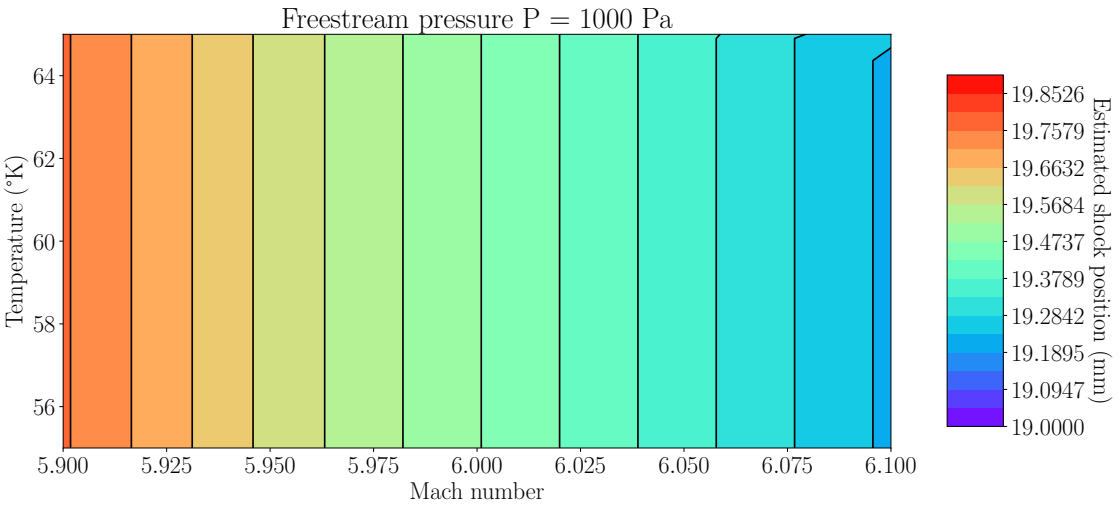

Fig. 7 Dependence of the shock position with free-stream temperature and Mach number at P_∞ = 1000 Pa

evaluated using this function at an arbitrary free-stream pressure are presented in figure 6. To get a rough estimate of the values of the correction coefficient when dealing with input quantities slightly out of the testing envelope which can be encountered during the convergence of the different algorithms, some supplementary simulations were also performed out of the experimental boundaries ($M \in \{5.2, 6.6\}$, $P_0 \in \{5, 35\}$ bars, $T_0 \in \{350, 550\}$ K).

2. Mach number correlation

A way of measuring the Mach number is looking at the shock geometry around the pressure probe using the schlieren photography data. Far enough downstream and far from the boundary layer, the shock should be free of all viscous interactions and thus should be a straight conical shock. The shock angle μ can then be theoretically directly linked to the free-stream Mach number M of the flow:

$$M = \frac{1}{\sin(\mu)} \tag{3}$$

For the highly supersonic flow encountered in the H3 however, this formula is rather impractical, because the Mach number becomes extremely sensitive to the shock angle. For example, at Mach = 2, an uncertainty of ±1 degree on the angle translates into uncertainty of ±0.06 on the Mach number. However, at Mach = 6, the same uncertainty generates an uncertainty of ±0.5 on the Mach number. Furthermore, in the H3 the relatively small diameter of the core flow means

that the straight region of the shock is hardly visible. Over the probe, the shock remains slightly curved.

Thus, a correlation is built from CFD simulations between the free-stream Mach number and the shock geometry. However, to build such a correlation, the shock geometry must be reduced to a single real number. The easiest solution is to measure the normal distance of the shock from the probe surface at a given position along the probe body. The further from the nose tip, the further the shock is from the probe, and thus the smaller the uncertainty is on the shock position measurement on schlieren photographs. However, the shock interacts with the Pitot probe curved shock underneath the probe and with the nozzle boundary layer overhead (see figure 3). Therefore, the distance from the nose tip cannot be arbitrarily large. A good compromise is found at $x = 0.1$m from the ogive.

Since the the shock wave geometry depends to some extent on the boundary layer displacement thickness along the probe, we expect the shock position to be dependent on not only the Mach number but on all the flow parameters. Thus, the simulations performed in III.B.1 are reused by extracting the shock positions at $x = 0.1$m from the ogive. The shock position at a given position along the probe body is defined for the CFD simulations as the first ordinate y along the normal to the surface, starting from the free-stream, for which the density gradient is maximum. The results for some input parameters are shown in figure 7. The dependance on temperature is seen to be very tenuous for the pressure presented. However this is not the case for all pressures. The dependance in free-stream pressure and Mach number is in any case very strong.

C. Nozzle flow simulation

To provide a point of comparison for the experimental results, a series of second-order finite volume simulations of the entire nozzle and test section of the H3 are performed, using the CFD++ software. The probes themselves are not modeled. Those simulations are 2D-axisymmetric, and steady. The inlet boundary is an inflow condition, defining pressure and temperature corresponding to the experimental measurements. The complex behavior of the diffuser (described in [9]) is not modeled, instead the outlet boundary is set to a simple back pressure condition, at the estimated free-stream pressure. Walls of the nozzle are considered isothermal. The fluid is considered fully compressible, with a perfect-gas equation model for molecular interactions. A RANS 2-equations $k-\omega$ SST model for turbulence is chosen, with wall functions to estimate the behavior of the flow in the boundary layer.

D. Flow rebuilding methodologies

The different quantities and models at play in the flow rebuilding procedures are schematized in figure 9. The rebuilding procedures can be classified by their respective methodologies for the computation of the Mach number. There are four main procedures, two of which rely strongly on an isentropic assumption for the flow expansion on the nozzle, while the others do not, with the exception of the computation of the free-stream quantities for the viscous correction and shock position correlation. In all cases, the Mach number in the test section has been measured during the campaign and is not extracted from former characterization campaigns, CFD simulations, or other discrete methods.

One of the main hypotheses for the flow rebuilding is the axial symmetry of the flow. Since the Pitot sensor and the static pressure sensor are located at an identical distance from the longitudinal axis of the nozzle and also from the nozzle exit, the flow state around one probe can be considered identical to the other probe. Due to time constraints this was not verified in practice for the current test campaign by rotating the probes along the nozzle axis; however previous experimental investigations (e.g. in [9]) confirm the axisymmetry hypothesis for other probe configurations.

1. Mach number from Pitot pressure measurements

The first algorithm is the classic [9] rebuilding method for the H3 wind tunnel; its flowchart is presented in figure 10a. Here, the Mach number is inferred from the measurement of the Pitot pressure and the reservoir pressure, by solving equation (4) for M. This equation relies on the isentropic expansion of the flow in the nozzle.

$$\frac{P_{t2}}{P_0} = \left(\frac{(\gamma+1)M^2}{(\gamma-1)M^2+2}\right)^{\frac{\gamma}{\gamma-1}} \left(\frac{\gamma+1}{2\gamma M^2+1-\gamma}\right)^{\frac{1}{\gamma-1}} \tag{4}$$

The free-stream temperature is extrapolated from the reservoir temperature measurements. It is injected in the viscous correction, which can then be used to compare the static pressure probe output to the expected static pressure with the isentropic assumption, extrapolated from the reservoir pressure measurement.

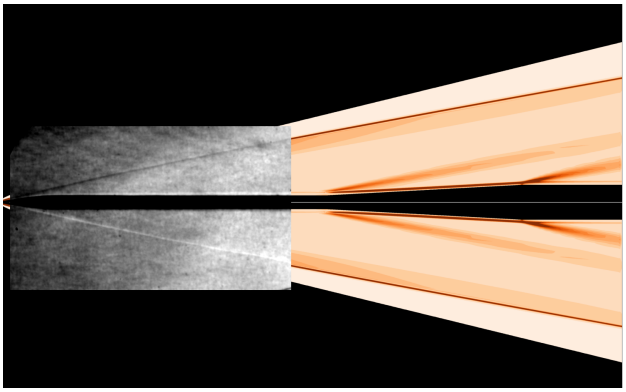

Fig. 8 Comparison of the schlieren visualization of an experimental run (P_0 = 10.7Pa, T_0 = 432.2K) and the CFD simulation the flow around the static pressure probe. The CFD simulation is run for M = 6 and at unit a Reynolds number similar to the experimental run. One can notice the slight difference in shock geometry, which indicates a Mach number different from 6 in the experimental run.

2. Mach number from static pressure measurements

The second algorithm is similar to the one presented in III.D.1. The Mach number is also computed using the reservoir pressure and the free-stream measurements, making use in this case of the free-stream static pressure probe with the help of equation (5). Since the viscous correction of this probe needs a measurement of the Mach number as an input, the algorithm is iterative. Its stopping condition is a difference in Mach numbers between two iterations close to machine precision. Its flowchart is shown in figure 10b.

$$\frac{P_\infty}{P_0} = \left(1 + \frac{(\gamma - 1)M^2}{2}\right)^{\frac{-\gamma}{\gamma-1}} \tag{5}$$

3. Mach number from both free-stream pressure measurements

The third method does not rely for the most part on an isentropic expansion assumption in the nozzle. Here, the Mach number is rebuilt from the ratio between measured Pitot pressure and static pressure measurements in the free-stream, using the Rayleigh-Pitot equation (shown in equation (6)). The algorithm is iterative, as the static pressure must be corrected for viscous effects using the Mach number. Its flowchart is presented in figure 10c.

$$\frac{P_{t2}}{P_\infty} = \left(\frac{(\gamma + 1)M^2}{2}\right)^{\frac{\gamma}{\gamma-1}} \left(\frac{\gamma + 1}{2\gamma M^2 + 1 - \gamma}\right)^{\frac{1}{\gamma-1}} \tag{6}$$

4. Mach number from schlieren photographs

Finally, another way of measuring the Mach number independently from the pressure probe measurements is to use the shock geometry, using the correlation described in section III.B.2 between the Mach number, free-stream pressure, free-stream temperature, and shock height at a chosen horizontal position along the static pressure probe. In figure 8, a visual comparison between CFD simulation of the flow around a probe for a flow at Mach = 6 and a schlieren photograph at a slightly different Mach number is presented; one can notice the slight discrepancy between the shock positions. The correlation is used to match the shock position and thus obtain the Mach number.

The shock position is extracted from the schlieren photographs using a Canny filter and a probabilistic Hough Line Transform for line detections. The parameters of those algorithms must be tweaked between the different runs, because of the variations in lighting conditions due to the sensitivity of the optical knife to the vibration of the tunnel.

The free-stream temperature and pressure are needed for the correlation and extrapolated using an isentropic expansion assumption of the nozzle. This algorithm is thus also iterative. Its flowchart is shown in figure 10d.

E. Condensation

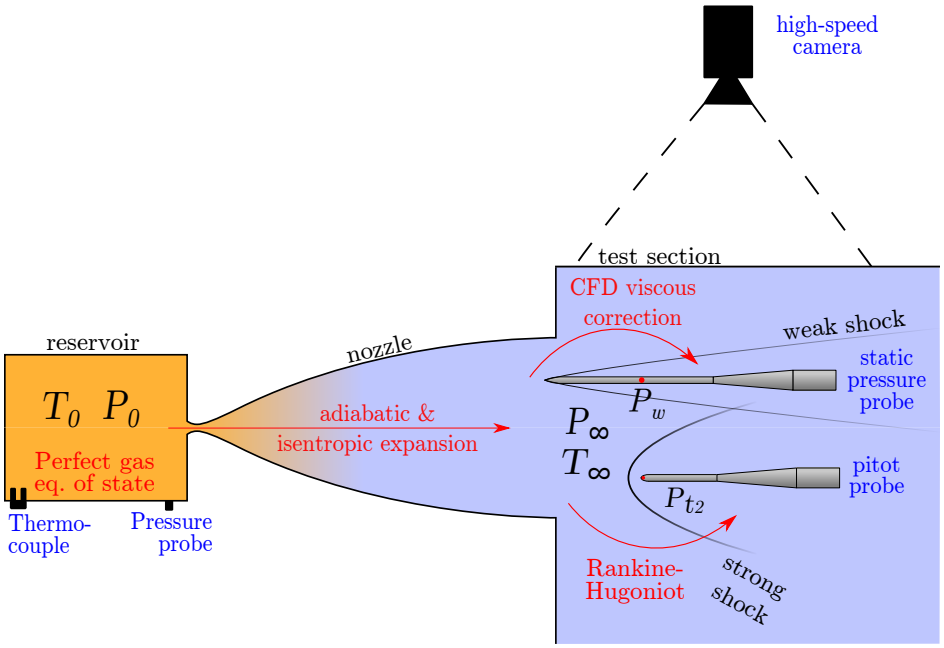

Fig. 9 Schematic of the main H3 rebuilding quantities and model. For clarity, the models and quantities linked to the schlieren measurement have been omitted.

1. Analytical correlation

Like in most cold hypersonic wind tunnels, the flow in the H3 can condense at low temperatures. The phenomenon has been historically observed on this particular tunnel; it even used to be as employed a seeding technique for qualitative laser sheet visualization.

In hypersonic tunnels, condensation is usually triggered at nitrogen saturation ratios superior to unity; this is the phenomenon known as supercooling. It can be predicted with an analytical correlation provided by Daum & Gyarmathy [4]. There are two main phenomena through which a liquid droplet can form: heterogeneous condensation initiated from a solid particle in the flow, and homogeneous condensation initiated from the fusion of small molecular clusters bound by Van der Walls forces.

Daum defines the nozzle expansion rate $\dot{P}$:

$$\dot{P} = -\frac{u}{p}\frac{\mathrm{d}p}{\mathrm{d}x} \tag{7}$$

For contoured nozzles such as the one of the H3, a correlation exists to compute this parameter:

$$\dot{P} = -\frac{1}{P_\infty}\frac{0.05u_\infty}{l} \tag{8}$$

In the H3, the expansion parameter remains inferior to 100 s^{-1}, which is small enough to consider heterogeneous condensation as the sole driving mechanism; consequently, the supercooling should not exceed a few Kelvins in terms of free-stream temperature.

The saturation condensation temperature in Kelvins for nitrogen is given by the following correlation:

$$T_s = \frac{336.4}{4.114 - \log_{10}(\frac{P_\infty}{P_{atm}})} \tag{9}$$

Daum & Gyarmathy provide a conservative relation between the supersaturation ratio S_c and the nozzle expansion rate $\dot{P}$ (Fig. 4), and finally the expected difference in temperature from the saturation line is given by the following relation:

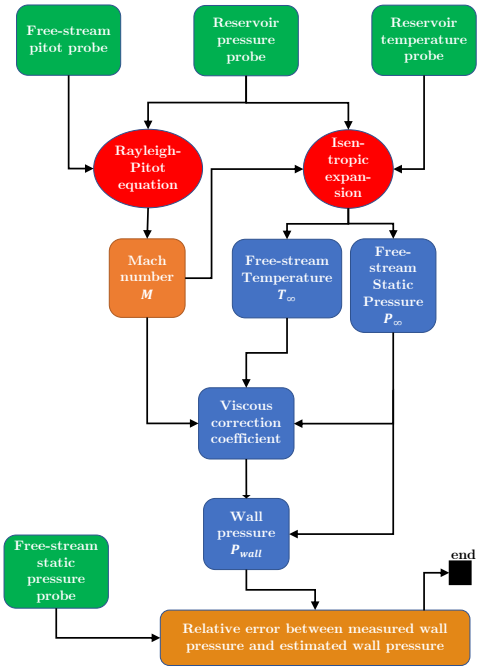

(a) Flowchart of the "Mach from Pitot pressure" rebuilding method.

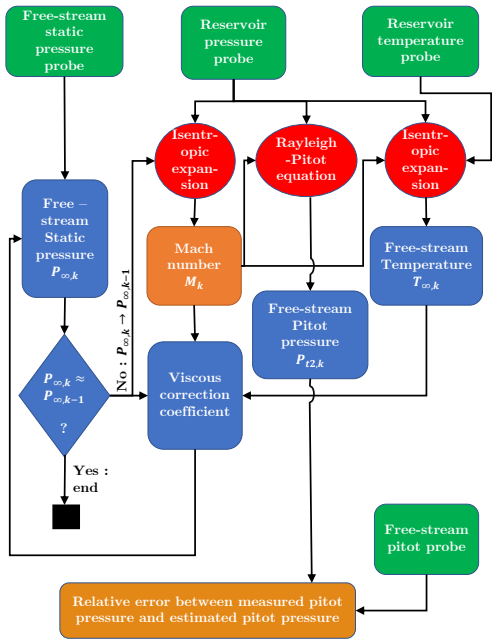

(b) Flowchart of the "Mach from static pressure" rebuilding method.

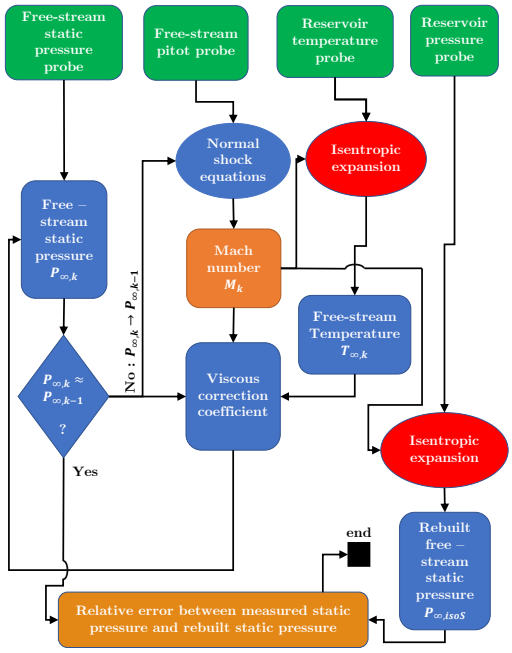

(c) Flowchart of the "Mach from free-stream pressures" rebuilding method.

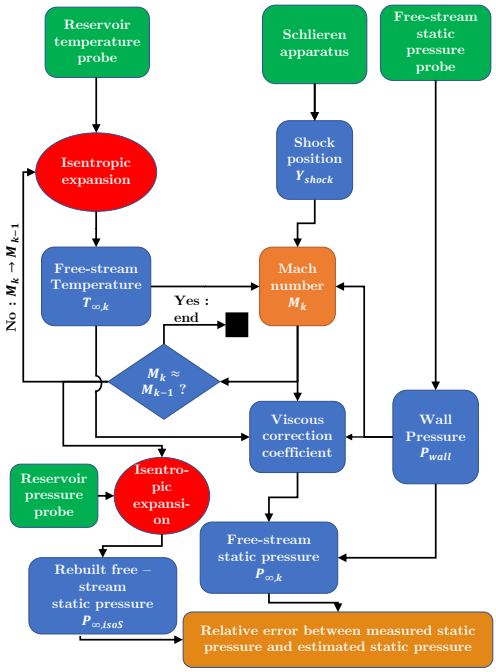

(d) Flowchart of the "Mach from schlieren visualization" rebuilding method.

Fig. 10 Flowcharts of the four different rebuilding algorithms. A square represents a quantity, a diamond represents a test and an oval represents a model. Experimental measurements are colored in green, an isentropic assumption for the flow expansion in the nozzle is flagged with the red color, and the output of the algorithm is marked in orange.

$$S_c = \frac{\frac{L}{RT_c}\frac{T_s - T_c}{T_s}}{\frac{4}{\rho_L}\left(\frac{\pi}{3m}\right)^{1/2}\left(\frac{\sigma}{RT_c}\right)^{1/2}} \tag{10}$$

where

- T_c is the supercooling condensation temperature
- T_s is the saturation condensation temperature
- m the mass of one molecule
- ρ_L the density of the liquid
- σ the viscosity of the liquid
- L the latent heat of condensation

2. Experimental detection method

Air condensation in the nozzle means that, at a given distance from the nozzle throat, the expansion stops following an isentrope curve in the pressure-temperature plane and follows a condensation curve. This translates into a higher static pressure in the free stream than the isentropic static pressure. Hence, the static pressure probe can be used to detect the condensation by plotting error in static pressure against temperature at constant reservoir pressure. A sharp change in the magnitude of the error below a given temperature should be interpreted as a sign of condensation.

The stagnation pressure in the free stream is also impacted by the non-isentropic expansion, but complex phenomena happening in the bow shock and the recompression region between the sensor and the shock in presence of liquid particles can render Pitot probes ineffective at detecting the condensation threshold, especially in low supersonic flows [5].

F. Uncertainty estimation

Uncertainty estimation on pressure and temperature data is performed using statistical analysis on the temporal evolution of the output of the probes. The flow state is supposed to be constant during each run, and each run is supposed to be long enough to acquire sufficient data to perform type-A uncertainty analysis. In practice, the number of data points collected for each run is limited by the relatively slow rate of acquisition of the thermocouple voltage but still amounts to about 200 points per run. The central value is thus the temporal mean and the uncertainty estimate is proportional to the standard deviation from this mean. These estimates have shown to be far superior to the sensors' respective uncertainties provided by their manufacturers, which are thus neglected.

The exception to this rule is the computation of uncertainties for schlieren measurements. As it would be too computationally complex to retrieve the Mach number from each image, only one standstill of the flow is extracted per run. The error estimation is then performed by estimating the thickness in pixels of the shock on the picture which translates to the error on the shock position estimation, for correctly-focused runs. Some runs, however, were performed slightly out of focus, for those the uncertainty is estimated by measuring the width of the blurred region on the probe edge. The width of shock and probe edges are considered constant throughout the runs. This is a conservative estimate; indeed the vertical position of the shock at a given abscissa is not gauged using solely schlieren data at the abscissa, but along the whole length of the probe when using the line detection algorithm. The actual uncertainty on the shock position value is consequently sub-pixel, but is not trivial to evaluate and thus a conservative approach has been chosen.

IV. Results

A. General presentation of the outcome of the test campaign

A test campaign was carried out over the span of 6 days, resulting in 67 runs. The testing envelope has four limits:

- The maximum feeding pressure of the supply line
- The minimum startup pressure of the H3
- The maximum power of the pebble bed heater
- The air condensation limit

Since one of the goals of the test campaign is to characterize experimentally the condensation limit, tests were performed in the vicinity, or even markedly below the analytical condensation temperature. The nature of the control system of the H3 makes it easy to regulate the reservoir pressure; however, the reservoir temperature is much more

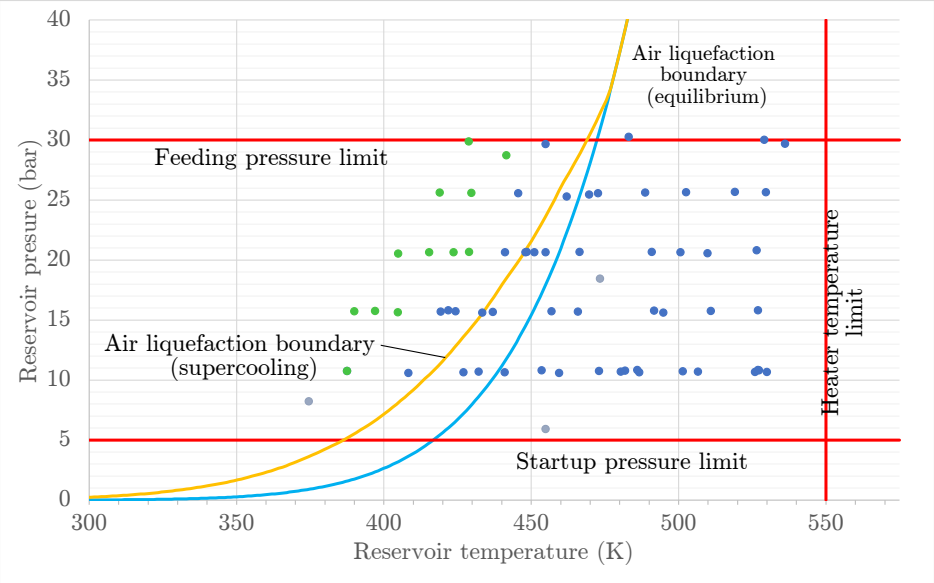

Fig. 11 Map of all the runs performed during the test campaign sorted by their measured reservoir pressure and temperature. Each individual run is indicated by a marker; blue for the runs with no condensation observed, green for runs with condensation, and gray for inconclusive runs. The red lines are the technical boundaries of the testing envelope. The blue curve corresponds to the theoretical condensation equilibrium of nitrogen at M = 6. The orange curve corresponds to the theoretical condensation threshold of nitrogen predicted by the supercooling theory [5] at M = 6.

unpredictable. Therefore, one can categorize the runs by reservoir pressure; 5 main classes of runs can be distinguished: 10 bars, 15 bars, 20 bars, 25 bars, and 30 bars. Two runs were performed below 10 bars, but the instability of the startup process of the tunnel at low pressures prevented further testing in this region of the operating map. All the runs and the boundaries of testing envelope are mapped on a reservoir pressure-temperature map in 11.

The qualitative good behavior of the flow around the instrumentation set up in the test section is assessed by a first look at the schlieren visualization. An example is shown in figure 3. The position of the respective shocks around the probes is downstream of the position of the sensor of the other instrument, ensuring that the presence of one probe cannot influence the behavior of the other. Furthermore, the boundary layer around both probes is visible. As expected, the boundary layer separates almost immediately from the Pitot probe, while around the more slender static pressure probe, the boundary layer remains attached, at least until the conic base.

Additionally, the sensitivity of the static pressure probe to a potential misalignment was investigated using the H3 incidence control system. Three runs at similar reservoir conditions ($P_0 = 10.75 \pm 0.04$ bars, $T_0 = 477 \pm 4$K) were performed at incidences of $\alpha = +2°$, $\alpha = -2°$ and $\alpha = 0°$. The difference in ratio between static pressure and reservoir pressure did not vary by more than 0.2%, and no separation of the boundary layer on the static pressure probe body could be detected using the schlieren visualization. This result is similar to other static pressure probes [1]. Given that an unintentional misalignment of the probes would be of much lower magnitude than +2°, this source of error can be eliminated.

B. Comparison of rebuilding methods

A comparison of the free-stream Mach numbers obtained using the different rebuilding algorithms is presented in figure 12.

The three methods making use of pressure probe measurements output markedly distinct Mach numbers, each falling outside of the uncertainty bars of the others, for all pressure and temperature conditions. The classic Pitot method, which uses an isentropic assumption for the flow expansion in the nozzle, outputs Mach numbers coherent with earlier Pitot-rake characterization works [2]. Notwithstanding, the method using the static pressure measurement in the free stream systematically outputs Mach numbers about 2 or 3% lower, whereas the method of measuring the Mach number using only the free-stream measurements outputs a markedly lower estimation, with a difference of the order of 10%

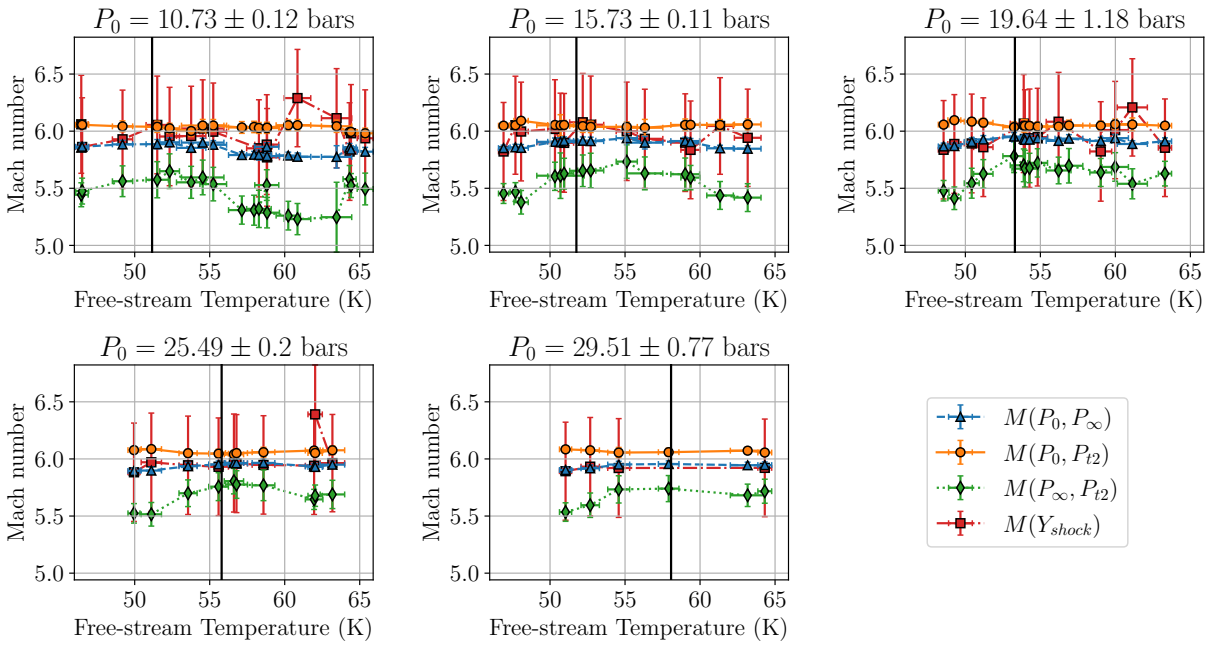

Fig. 12 Free-stream Mach numbers evolution with free-stream static temperature for different reservoir pressures. The thick black vertical lines represent the analytical condensation limit computed with Daum's theory of supercooling. The algorithms used for the determination of each of these Mach numbers are described in section II. Uncertainty bars are shown for a 95% confidence interval.

from the Pitot isentropic estimation.

The measurement of the free-stream Mach number using schlieren data must be considered separately. The relatively high uncertainty of this measurement procedure makes it unfit for a one-by-one comparison with the other methods. Nonetheless, one can note that the fully free-stream measurement method falls on the edge or outside the uncertainty bars of the schlieren measurement method, for every isobaric data series. Furthermore, the mean estimate falls systematically very close to the output of the isentropic methods (static and Pitot). Knowing that, as discussed in III.F, the uncertainty is probably overestimated, we have strong hints that the output of the fully-free stream method is not compatible with the others.

A first interpretation for the discrepancy between Mach measurements from the "Mach from Pitot pressure" and "Mach from static pressure" methods is the presence of non-isentropic phenomena occurring in the H3 nozzle, to which the static pressure probe is more sensitive than the Pitot probe, the relatively low heat, and pressure conditions in the reservoir of the H3 ruling out any high-temperature effect on the sensor. This would be a similar result, to the Longshot experiments performed by Grossir [1], albeit with a much lower magnitude of discrepancy. This is however surprising, because of the relatively low hypersonic Mach number of the H3 nozzle; all possible physical interpretations for the discrepancies observed in the Longshot rely on high Mach numbers, or high temperature and pressure effects in the reservoir. Therefore, a second interpretation must be considered: the calibration of the static pressure probe, in particular the viscous correction applied to its output, does not correspond to reality. There are several possible sources of error. The first is the presence of turbulence in the boundary layer around the probe. The viscous correction has been built with a laminar hypothesis.

A sample fully turbulent simulation of the flow around the static pressure probe is performed using a RANS $k-\omega$ SST model with turbulence quantities solved to the wall ($y^+_{\max} = 0.25$, no wall functions are used). The result shows a slightly superior ratio between the free-stream pressure and the wall pressure value at the sensor position, with a 0.8 percentage point difference between fully laminar and fully turbulent simulation. This is within the experimental uncertainty, but markedly superior to the variation between laminar simulations over the testing envelope. To investigate the nature of the flow in the boundary layer around the probe, some runs were performed with a close-up of the high-speed camera on the probe boundary layer, allowing for a higher acquisition rate. The succession of images is

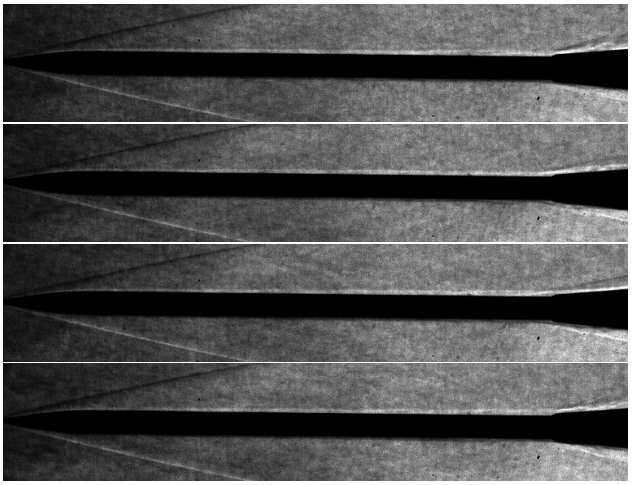

Fig. 13 Schlieren photographs of the static pressure probe. These shots are separated by 40 µs; their exposure time is 2.02 µs. The run was performed at P_0 = 30.28 bars and T_0 = 483.09 K. Instabilities in the boundary layer can be seen in the region of the conical base, and also more faintly on the leftmost part of the needle. The gain, brightness, and gamma of the image have been adjusted to highlight the boundary layer.

shown in figure 13. While instabilities visibly appear over the conical base probe, no hints of turbulence, or transition to turbulence, can be found in the vicinity of the pressure intakes of the sensor. The boundary layer is thus probably not fully turbulent, and in particular not around the sensor. However, in the boundary layer, phenomena occurring downstream can influence the flow upstream. A related source of error is the geometry of the junction between the conical base of the probe and the needle, which has a non-negligible soldering thickness not modeled in the mesh used for the viscous correction. The presence of this small element could translate into an overpressure region near the conical base of higher magnitude than expected, which directly influences the pressure ratio in the vicinity of the sensor.

A focus on the results for the 25 bars pressure series is shown in figure 14, on which the estimated Mach numbers at the probe position estimated using results of the CFD simulations of the nozzle described in III.C are plotted for comparison. The CFD results are coherent with the "Mach from Pitot pressure" rebuilding algorithm. This is a further confirmation of the reliability of the Pitot probes measurement; however, no conclusion can be made on the presence or absence of non-isentropic phenomena in the nozzle, since such effects are not introduced in CFD simulations and Pitot probes are known to be insensitive to those phenomena.

C. Detection of condensation

The evolution with the free-stream temperature of the relative error between the measured static pressure and the static pressure extrapolated from reservoir measurements using an isentropic expansion assumption in the nozzle is plotted in figure 15 along with the analytical condensation temperature. The Mach number used in the expansion model is calculated using the ratio between the measured Pitot and reservoir pressures.

For each reservoir pressure series, a sharp rise in error can be observed below a given temperature. This is coherent with the presence of condensation at those temperatures: measured static pressure becomes very superior to the isentropic pressure. The chosen condensation detection threshold is, for a given isobaric series, the first run below which the error in static pressure rises with temperature (in the vicinity of the analytic condensation onset). As expected, supercooling is observed : all points for which condensation is detected are below the saturation temperature of nitrogen. The supercooling effect is even slightly more intense than predicted by Daum's theory; which is not surprising since a conservative relation between the saturation coefficient and the nozzle expansion rate has been chosen. In figure 11, the points for which condensation has been detected experimentally are marked in green. These results should be taken with caution, as there is relatively high uncertainty in the measurement of the temperature at the outset of this rise. It is not possible to guarantee a total absence of condensation for the points in the neighborhood of the experimental limit. Even so, the condensation onset seems steadily below the previously used saturation line. This opens the testing envelope of the H3; a lower temperature at equal pressure means s higher unit Reynolds number available. The new

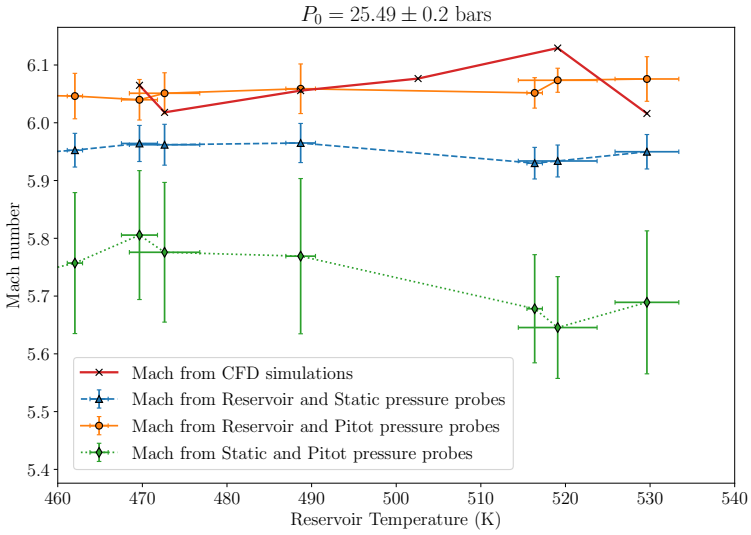

Fig. 14 Free-stream Mach number evolution with reservoir temperature for runs at 25 bars of reservoir pressure. The algorithms used for the experimental determination of each of these Mach numbers are described in section II and the nozzle flow simulations are described in section III.C. Uncertainty bars are shown for a 95% confidence interval.

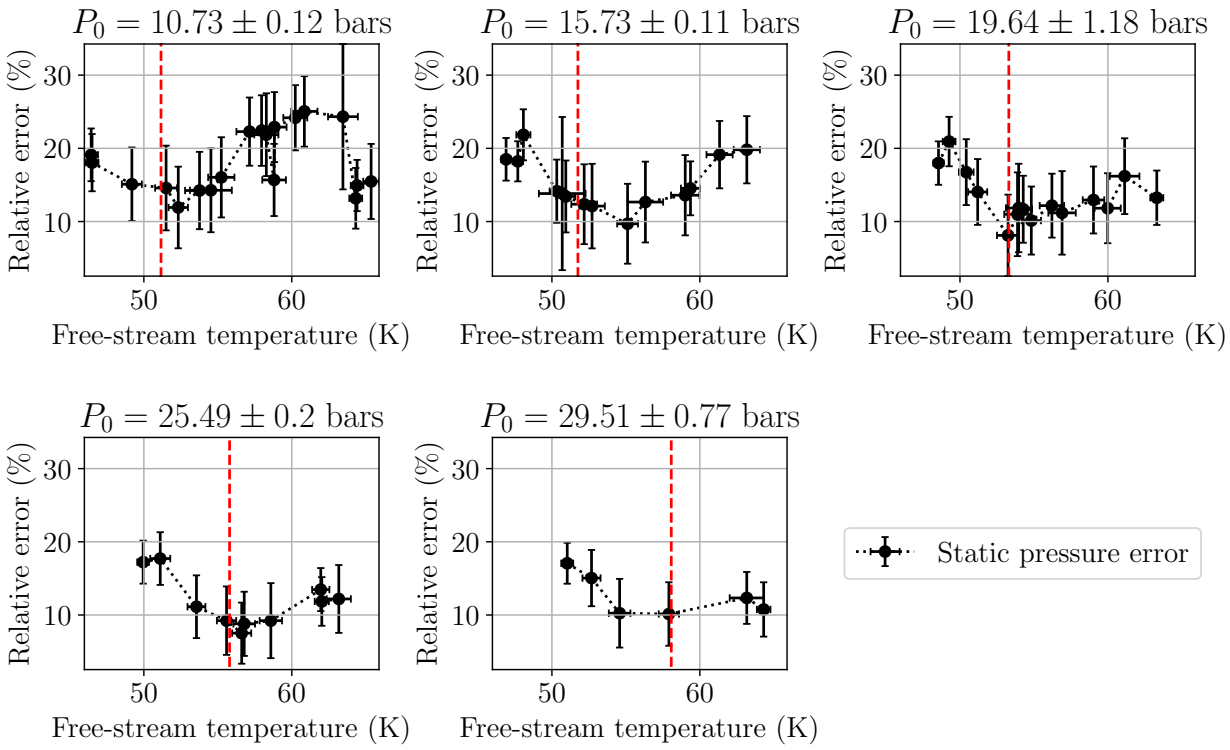

Fig. 15 Evolution with the free-stream temperature of the relative error between the direct measurement and the values extrapolated from reservoir conditions of the static pressure in the free stream plotted for different reservoir pressures. The Mach number for isentropic extrapolation is obtained from the ratio between Pitot pressure measurements and reservoir pressure measurements. The vertical red lines correspond to the analytical air liquefaction limit (with supercooling) for each reservoir pressure [5]. Uncertainty bars are shown for a 95% confidence interval.

maximum unit Reynolds number of the H3 is about $3.0E7$ m^{-1}, while it previously was of the order of $2.7E7$ m^{-1}.

D. Possible improvements for future test campaigns

There are several ways through which this characterization campaign could be improved, which would allow to conclude on whether the discrepancy observed in the static pressure measurements in the current analysis comes from experimental error or the presence of non-isentropic phenomena in the boundary layer. First, the presence of a third probe in the free-stream could enable the direct measurement of the free-stream Reynolds number. Hot-wire anemometry or cold-wire thermometry are both potential candidates. This would allow a direct viscous correction of static pressure measurements and Mach number measurements from schlieren, avoiding any reliance on the reservoir measurements.

However, CFD simulations showed that the static pressure correction was only moderately dependent on the testing conditions, with an overall difference of less than a percentage point over the whole test envelope. Thus, it is unlikely that a more reliable measurement of the free-stream quantities number would decisively change the conclusion of the analysis, even if it could give more confidence in the results. Nevertheless, there are strong hints that the CFD simulations themselves have a great margin of progression. The presence of some instabilities in the boundary layer at the aft of the probe and the difference in geometry between the probe and its numerical model at the junction are both crucial discrepancies between the CFD simulations and experiments that should be reduced.

Other possible robustness checks for the free-stream pressure sensing are listed below :

- Running tests with only one probe in the test section to check for possible cross-influence phenomena between the probes, (even if the current shock geometry makes such an eventuality unlikely). For the same reason, a simulation of the complete test section, including the Pitot probe and the Static pressure probe, using inlet data from a separate nozzle simulation, could increase the confidence in the viscous correction.
- Running tests at different distances from the longitudinal axis of the nozzle to assess the sensitivity of the static pressure probe output to the distance from the nozzle boundary layer

Furthermore, the schlieren Mach number measurement uncertainty can be greatly reduced by the usage of a higher-definition camera. In the current analysis, the usage of a high-speed camera warranted the detection of short-lived flow disturbances but was detrimental to the overall quality of a standstill image. Using for example a classic reflex camera could dramatically reduce the width of a pixel and thus the error on the shock position measurement.

Finally, a completely different approach to the calibration of the static pressure probe would be to use it in parallel with another static pressure probe which has been characterized reliably. This would help validate the CFD modeling of the flow around the probe and give more confidence in the experimental results. To this end, it might be possible to use the Longshot static pressure probes designed by Grossir [1] which are still in good operating condition. However, the small test section of the H3 might render such tests unfeasible; the wider Longshot test section seems more appropriate but the higher Mach number makes any translation of the validation of the CFD modeling in the Longshot to the H3 test section quite hazardous.

V. Conclusions

An extensive characterization test campaign has been carried out in the H3 wind tunnel, using intrusive free-stream static pressure and Pitot probes, as well as schlieren measurements. The wind tunnel was tested over its entire operating map. CFD simulations were run to correct the static pressure probe readings for viscous effects and compute the Mach number from the geometry of the shock around the static pressure probe. The Pitot measurements were found to be in adequation with earlier results, but the static pressure probe measurements showed a lower Mach number than expected for an isentropic expansion of the flow in the nozzle.

The cause of this discrepancy in Mach number, of about 3%, has two possible explanations. The first, and most probable, is an error in the viscous correction of the pressure measurement, which can be caused by slight differences between the probe and its numerical model. The second is the presence of non-isentropic effects in the nozzle, similar to the phenomena observed in the von Karman Institute's Longshot tunnel nozzle [1]. Unlike the Longshot study, however, the lesser magnitude of the discrepancy renders schlieren visualization incapable of deciding which measurement among the Pitot and the static pressure probe rebuilds the accurate Mach number; the uncertainty on the shock position used to rebuild the Mach number from the schlieren photographs is too high for such conclusions. It is, nonetheless, sufficiently low to rule out the free-stream method for the computation of the Mach number, which means that the discrepancy observed cannot originates from a faulty reservoir pressure measurement.

While the accuracy of the absolute measurement of the static pressure remains equivocal, the evolution of this error throughout the operating map of the wind tunnel has been used efficiently to detect condensation. The experimental

condensation was measured at lower temperatures than predicted by the nitrogen saturation previously used, and even slightly below the temperatures predicted by the theory of supercooling. This enlarges the H3 operating map, which can prove useful for future test campaigns.
The main shortcoming of this study is the partial free-stream characterization of the flow. A supplementary probe measuring mass flow or heat fluxes would ensure that no reservoir data has to be used to compute the free-stream quantities and thus the viscous correction of the static pressure probe. Furthermore, this third intrusive measurement could be used to rebuild the Mach number using a distinct algorithm; this would advantageously replace the schlieren visualization as a way of validating the Pitot or the static pressure measurements since a lower uncertainty is expected.

Acknowledgments

The authors wish to thank MM. T. Boeyen, P. Collin, S. Paris, D.Kovács, M. Spillemaekers, and A. F. Torre for their precious help in the conduct of study.

References

[1] Grossir, G., Van Hove, B., Paris, S., Rambaud, P., and Chazot, O., "Free-stream static pressure measurements in the Longshot hypersonic wind tunnel and sensitivity analysis," *Experiments in Fluids*, Vol. 57, No. 5, 2016, p. 64. https://doi.org/10.1007/s00348-016-2137-5, URL https://doi.org/10.1007/s00348-016-2137-5.

[2] Masutti, D., Spinosa, E., Chazot, O., and Carbonaro, M., "Disturbance Level Characterization of a Hypersonic Blowdown Facility," *AIAA Journal*, Vol. 50, No. 12, 2012, pp. 2720–2730. https://doi.org/10.2514/1.J051502, URL https://doi.org/10.2514/1.J051502, publisher: American Institute of Aeronautics and Astronautics.

[3] Fay, J. A., and Riddell, F. R., "Theory of Stagnation Point Heat Transfer in Dissociated Air," *Journal of the Aerospace Sciences*, Vol. 25, No. 2, 1958, pp. 73–85. https://doi.org/10.2514/8.7517, URL https://doi.org/10.2514/8.7517, publisher: American Institute of Aeronautics and Astronautics.

[4] Daum, F. L., and Gyarmathy, G., "Condensation of air and nitrogen in hypersonic wind tunnels." *AIAA Journal*, 1968. https://doi.org/10.2514/3.4520, URL https://arc.aiaa.org/doi/abs/10.2514/3.4520.

[5] Daum, F. L., "Air condensation in a hypersonic wind tunnel," *AIAA Journal*, Vol. 1, No. 5, 1963, pp. 1043–1046. https://doi.org/10.2514/3.1722, URL https://doi.org/10.2514/3.1722, publisher: American Institute of Aeronautics and Astronautics.

[6] Wegener, P., and Mack, L., "Condensation in Supersonic and Hypersonic Wind Tunnels," *Advances in Applied Mechanics*, Vol. 5, Elsevier, 1958, pp. 307–447. https://doi.org/10.1016/S0065-2156(08)70022-X, URL https://linkinghub.elsevier.com/retrieve/pii/S006521560870022X.

[7] Nagamatsu, H. T., Geiger, R. E., and Sheer, R. E., "Real Gas Effects in Flow over Blunt Bodies at Hypersonic Speeds," *Journal of the Aerospace Sciences*, Vol. 27, No. 4, 1960, pp. 241–251. https://doi.org/10.2514/8.8494, URL https://doi.org/10.2514/8.8494, publisher: American Institute of Aeronautics and Astronautics.

[8] Behrens, W., "Viscous interaction effects on a static pressure probe at M equals 6," *AIAA Journal*, Vol. 1, No. 12, 1963, pp. 2864–2866. https://doi.org/10.2514/3.2193, URL https://arc.aiaa.org/doi/10.2514/3.2193.

[9] Agostinelli, P. W., Turchi, A., Quang, D. L., Masutti, D., Vigevano, L., D'Ambrosio, D., and Chazot, O., "Investigation of Hypersonic Flow in the VKI H3 Wind Tunnel: from Facility Characterization to Boundary-Layer Interaction over Low-Temperature Ablators," *23rd AIAA International Space Planes and Hypersonic Systems and Technologies Conference*, American Institute of Aeronautics and Astronautics, 2020. https://doi.org/10.2514/6.2020-2445, URL https://arc.aiaa.org/doi/abs/10.2514/6.2020-2445.